

# Characterization of the Time of Phytosanitary Treatment of Frozen or Unfrozen Wood by Microwaves



F. Erchiqui and H. Kaddami

**Abstract** The traffic and transportation of wood products around the world is one of the causes that have facilitated the migration of pathogens and insects between countries. These biological invasions have resulted in the destruction of plant species, causing significant economic and ecological losses in many parts of the world. To this end, the World Trade Organization, through the International Plant Protection Convention Working Group, has established a standard for phytosanitary measures (ISPM 15), which requires that wood products (pallets, packaging, etc.) be treated according to this standard. It is within this framework that this chapter is included and aims to present a numerical approach to quantify the time required for microwave phytosanitary treatment of wood products. For this purpose, the microwave heat conduction equation is expressed in terms of volumetric enthalpy and numerical resolution is achieved using the finite element method. As an application, we considered three Canadian wooden. For the analysis, we considered a frequency of 2466 MHz, temperatures from  $-20$  to  $+20$  °C and a moisture content of 131%.

**Keywords** Phytosanitary treatment · Microwave · Orthotropic media · Thermal anisotropy · Enthalpy · Dielectric anisotropy · Finite element analysis

## 1 Introduction

Circulations of some wood products are identified as one of the dissemination vectors and spread of non-native pathogens and insects in several countries of the world. This biological invasion has caused the destruction of plant species, causing significant economic and ecological disasters in many regions of the world. The Millennium

---

F. Erchiqui (✉)

School of Engineering, Bioplasturgy Laboratory, University of Quebec in Abitibi-Temiscamingue, Université, Rouyn-Noranda, 445 boul, Québec, Canada  
e-mail: [fouad.erchiqui@uqat.ca](mailto:fouad.erchiqui@uqat.ca)

H. Kaddami

Department of Chemistry, Laboratory of Organometallic and Macromolecular Chemistry, FST-Marrakech, Cadi Ayyad University, Avenue Abdelkrim Elkhattabi, B.P. 549, Marrakech, Morocco

Ecosystem Assessment classifies them as one of the main causes of biodiversity loss, along with other factors, such as habitat destruction, climate change and pollution. For example, the North American forest (its extern part) is still endangered by the non-native Asian long-horned beetle (*Anoplophora glabripennis*) and the emerald ash borer (*Agrilus planipennis*) (USDA 2003). According to the Food and Agriculture Organization (FAO), this invasion is due mainly the combined effects of the climate change and wide traffic of packaged products. In addition, the devastating risks of these species invasion, which involve many interactions between various spatial and temporal parameters, are difficult to quantify (Yemshanov et al. 2009). Recent estimates of the global economic impacts of these species exceed US\$120 billion annually; this includes agricultural, forestry and public health impacts (USDA 2003). In Canada, the economic impact on the agriculture and forestry sectors has been estimated at Can \$7.5 billion annually (Yemshanov et al. 2009). To face this new global reality, the International Plant Protection Convention (IPPC) working group promulgated the “International Standards for Phytosanitary Measures 15 (ISPM 15)” regulation in 2009 on the treatment of phytosanitary of all wood and wood-based materials. This standard aims to protect ozone layer and thus forbids polluting and fights against the international dissemination and spread of pathogens, fungi and insects that could endanger agricultures or ecosystems (FAO 2009; Fields et al. 2002). Thereby, ISPM-15 imposed and authorized thermal and chemical treatments of the circulating woods and packaging materials to destructs these pathogens (FAO 2009). Nevertheless, these treatments have economical and ecological side effects and drawbacks. For example Cooper et al. have pointed out the issue of recycling of these materials by raising out the health impact of reusing chemically sanitized wood and wood based materials (Cooper et al. 1996): What is the health hazard to burn borate or Imidacloprid sanitized firewood? What is the generated environmental impact and health hazard if chemically treated materials are recycled for application in outdoor conditions where are subjected to rainfall and sunlight (Nzokou et al. 2008a, b)?

Dielectric heating treatment was ratified in ISPM 15 In 2013. It was proven that this heating technique is very effective in destroying pathogens (Nzokou et al. 2008a, b). Nevertheless, ISPM-15 has indorsed 56 °C as minimum temperature to destroy pathogens in piece of wood thicker than 6 mm when using this technique.

In regard of the heating efficiency of this technique, one of the major advantages is the production of heat inside the material in a short period of time (Norimoto and Gril 1989), (Gašparík and Barčík 2013, 2014), (Oloyede and Groombridge 2000), (Hansson and Antti 2003). Nevertheless, the assessment of the heat distribution generated by dielectric heating in wood and the prediction of the time of its phytosanitary treatment is a very hard task. Indeed, these predictions are tributary to many parameters such as (i) the non-isotropic dielectric, mechanical and thermal properties of wood, (ii) the product geometry and design, and (iii) its initial temperature and humidity, etc. Moreover, considering the diversity of wood based commercial products how is it possible to make sure of the total destroying of pathogens by dielectric heating treatment? At this stage, several uncertainties concerning the efficiency of such a treatment eliminating pathogens are to be checked. Thus, numerical

simulation and modeling in predicting the processing time become challenging. In these conditions, a multi-physical model is needed for these simulation and modeling and its effectiveness is directly related to how mathematically Maxwell's equations are coupled to conservation equations for wood? (Brodie 2007; Rattanadecho and Suwannapum 2009; Erchiqui et al. 2013; Erchiqui 2013a, b; Rattanadecho 2006; Zhu et al. 2007; Ni and Datta 2002). This raises a big challenge for numerical simulation since this has to consider the combined intricacies of mass and heat transfers, phase change as well as thermomechanical and electromagnetic interactions of a highly hygroscopic, thermally weak conductive and structurally anisotropy material as wood (Torgovnikov 1993; Norimoto and Yamada 1971). Several models are tested in literature to face these major challenges. The empirical model of Beer-Lambert is one of the most used models for Maxwell's equations. This model is valid for semi-infinite medium and can quantify the microwaves energy loss in irradiated material (Erchiqui et al. 2013). Thus, an extensive question evolves: To which extend this model is still applicable for wood considered as finished anisotropic medium. In the case of microwaves as well as for radiofrequency, a criterion of applicability is provided in (Zhu et al. 2007; Erchiqui 2013a, b). This defines a critical thickness of wood sample to respect by considering the penetration depth (cm) of the radiation inside the sample. However, in the case of frozen wood, the ice melting (phase change) during microwave heating should be considered, especially in this case when the medium is considered as anisotropic. This evolves a difficult question from numerical modeling vantage point since one or more moving boundaries are to be considered. To overcome this issue, two ways can be used, in general: resolving independently the equations of energy for the liquid and solid phases, and considering the moving solid-liquid interface (Hu and Argyropoulos 1995a, b; Panrie et al. 1991), or resolving the enthalpy function considered as the equation of energy (Erchiqui et al. 2013). On the other hand, when a phase change is to be considered, several modeling approaches could be found in literature in the area of wood and food sciences (Ohlsson and Bengston 1971; Swami 1982; Rattanadecho 2006; Bhattacharya et al. 2002; Basak and Ayappa 1997; Coleman 1990).

In the present work, which is a synthesis of work we carried out recently, we are treating the phytosanitary treatment of anisotropic frozen wood microwaves heating in order to numerically determine the time of application this kind of dielectric heating. To this end, a finite element 3D approach, involving the enthalpy-volume energy is elaborated. On the other hand, the wood sample is considered of parallelepiped geometry and the incident microwaves are plan and oriented perpendicularly to its faces. For such purpose, three Canadian wood species with different physico-chemical properties have been studied: trembling aspen (*Populus tremuloides* Michx), white birch (*Betula papyrifera*) and sugar maple (*Acer saccharum*).

## 2 General Considerations

We assume that in this work the treatment by microwave of the wood species does not induce the degradation of its physical and mechanical properties. This aspect will be considered in this work since the highest temperatures that will be reached are far below the degradation temperature of wood. On the other hand, the focus will be on the numerical modeling aspect, through the consideration of nonlinear thermo-physical and electrical properties. Also, the influence of the mass transfer will not be taken into account in this modeling work. The nonlinear heat conduction problem involving phase changes such as wood freezing is solved using three-dimensional volumetric specific enthalpy based on finite-element analysis. This study focused on a sample cube of wood 22 mm thick. We chose a moisture content of 131% for which the freezing phenomenon is pronounced. The choice of this high moisture content made the modeling process more delicate to handle with since one has to deal with water melting (phase change) during the heating process. The samples considered in this study derive from the external zone of the trunk (see Fig. 1). This choice is justified by geometrical considerations since for this part of the trunk one can easily make the assumption of cylindrical coordinates. On the other hand, this part of the wood (sapwood) is considered to have the tree's storage function. This part of the wood, which is wanted by microorganisms and insects, is frequently subjected to pathogen attack, in contrast to the heartwood, which has a relatively natural resistance to attack by microorganisms owing to the extractives that are stored within its dead cells (disposal site for harmful by-products of cellular metabolism).

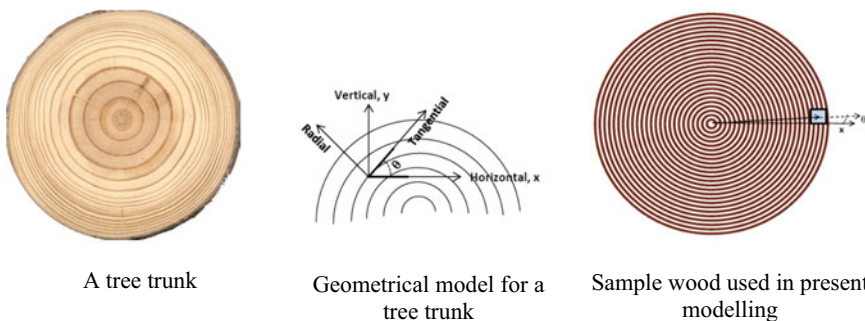


**Fig. 1** Wood sample's cross section with illustrations the angle of the ring curves and of the radial and angular position

### 3 Thermal Properties of Wood

Three principal thermal conductive properties, namely thermal conductivity, specific heat and thermal diffusivity, are to be considered when modeling the heat process of wood. Generally, all three properties vary with the specific gravity SG, based on dry mass and green volume, the wood moisture content MC, expressed as a percentage/fraction of the oven-dry mass of the wood and the temperature T. However, the ring orientation on a wood sample has a considerable effect on the rate of heat transfer. An example of a wood sample with curved rings is shown in Fig. 1. The two directions x and y shown in this figure are not exactly radial and tangential directions as defined by the wood anatomical structure; they will be called vertical and horizontal directions in the following. Accordingly, thermal conductivities in both directions on wood samples are usually different from the true radial and tangential direction. However, the thermal conductivities in the x and y directions can be calculated from the following formula:

$$k_x = -k_r \sin \theta + k_t \cos \theta \text{ and } k_y = k_r \cos \theta + k_t \sin \theta \quad (1)$$

Obviously, the thermal conductivity values change with the location, the  $\theta$  angle and the radial position  $r$  of the sample. For illustrative purposes, one average angle, defined at the center of mass of the sample relative to the x-axis, is considered. For heat transfer analysis, we consider an angular position close to zero (see Fig. 1). Under these conditions, we have:  $k_x \cong k_t$ ,  $k_y \cong k_r$  and  $k_z = k_t$ . The analytical expressions of the thermal conductivity, in the radial direction of the wood material, according to Kanter, are given in (Steinhagen and Harry 1988). The dependence of the thermal conductivity on temperature is generally low; it increases from 2 to 3% by 10 deg. For several species of wood, the ratio of longitudinal (kL) versus radial (kR) thermal conductivity is around 1.75 and 2.2, while the tangential thermal conductivity (kT) is usually slightly smaller (0.9 to 0.95 times) than the radial conductivity (Kanter 1975; USDA 1977).

The specific heat capacity of wood, Cp, which represents the thermal energy required to produce one-unit change of temperature in one unit of mass, is sensitive to humidity. The presence of water improves the specific heat of the wood because the specific heat of the water is greater than that of the wood.

For specific heat capacity, Cp, which represents the thermal energy required to produce one unit change of temperature in one unit of mass, an increase in moisture improves the specific heat of the wood because the specific heat of the water is greater than that of the wood. The analytical expressions, according to Steinhagen, are given in (Steinhagen and Harry 1988).

Thermal diffusivity, which is a measure of how rapidly a material can absorb heat from its surroundings, is related to thermal conductivity, specific heat capacity and density (Kanter 1975; USDA 1977). Density ( $\text{kg/m}^3$ ), which represents the weight of wood divided by the volume at a given moisture content, is one of the most important physical properties. The analytical expression for density considered in this work is that given in (Simpson and Tenwolde 1999).

Finally, to study wood heating (thawing or not), it is important to quantify the value of the latent heat of wood species. For this purpose, we can use the formula provided by Chudinov (1965):

$$L = L_w \left( \frac{MC - 30\%}{MC + 100\%} \right) \quad (2)$$

$L_w$  is the latent heat of water fusion (334 kJ/kg).

## 4 Complex Dielectric Properties of Wood

Propagation of electromagnetic waves in materials is determined by their electrical and dielectric parameters. In the case of dielectrics, the parameter of greatest interest is the complex permittivity,  $\varepsilon (= \hat{\varepsilon} - j\varepsilon'')$ , where  $j = \sqrt{-1}$ . This parameter describes the ability of the material to support an electric field: the real part of  $\varepsilon$ , known as the dielectric constant, describes the ability of a material to store energy and the imaginary part of the  $\varepsilon$ , known as the loss factor, describes the ability of a material to dissipate energy, which naturally results in heat generation. Usually, depending on the type of material, the permittivity varies with each phase of the material, since the concentration of molecules and their bonding in the material differ. Several theories have been proposed to describe the permittivity of dielectrics from the constituent elements, concentration and particle size and shape (Zielonka and Gierlik 1999; Phillips et al. 2001). For wood material, complex permittivity varies with the type of wood species, density, frequency, moisture content, temperature and structural orientation. From the electromagnetic point of view, it is desirable to refer to the complex *relative permittivity*,  $\varepsilon_r$ , as being its permittivity with respect to that of free space,  $\varepsilon_0$ , such that  $\varepsilon = \varepsilon_r \varepsilon_0$ .

For wood material, according to (Peyskens et al. 1984), the values of the longitudinal dielectric constant ( $\varepsilon_L$ ) are 1.25–3 times higher than the tangential dielectric constant ones ( $\varepsilon_T$ ), while the ratio of the tangential versus radial dielectric constant ( $\varepsilon_R$ ) is about 0.9 and 1.25.

With regard to the interactions between the material and the electric field, two physical parameters are of primary interest: the absorption and storage of electric potential energy within the dielectric material, and the dissipation or loss of part of this energy when the electric field is removed (James 1975). This dissipation of energy in the material induces effects on heat and mass transfer. To this end, note that the conductive heat process by microwave energy in different directions of wood has two important characteristics: (i) the amplitude of the oscillation of electromagnetic power distribution and (ii) the magnitude of the heat transfer rate. A rigorous mathematical formulation of the heating process requires a good knowledge of the power flux (Poynting vector) associated with electromagnetic microwave propagation, which is a solution of Maxwell's equation in anisotropic dielectric material.

For anisotropic dielectric wood, both the electric charge density ( $\rho$ ) and the electric currents ( $\mathbf{J}$ ) are equal to zero. Furthermore, the following linear interrelations can be established between the electric and magnetic properties (Pozar 2011):

$$\mathbf{D} = \overline{\overline{\epsilon}} \cdot \mathbf{E} \text{ and } \mathbf{B} = \overline{\overline{\mu}} \cdot \mathbf{H} \tag{3}$$

where  $\mathbf{E}$ ,  $\mathbf{B}$ ,  $\mathbf{H}$ , and  $\mathbf{D}$  are the electric field ( $\text{V m}^{-1}$ ), the magnetic field ( $\text{Wb m}^{-2}$ ), the magnetic induction ( $\text{A m}^{-1}$ ), and the electric displacement ( $\text{C m}^{-2}$ ), respectively.  $\overline{\overline{\epsilon}}$  and  $\overline{\overline{\mu}}$  are, respectively, the relative dielectric and permeability tensors. For wood, it is generally believed that the magnetic permeability tensor  $\overline{\overline{\mu}}$  is closely approximated by the real tensor  $\mu_0 \overline{\overline{\mathbf{I}}}$  ( $\overline{\overline{\mathbf{I}}}$  is the identity tensor) (Erchiqui 2013a, b).  $\mu_0$  (H/m) is the permeability of vacuum.

Rotation of the electric field vector  $\mathbf{E}$  on  $180^\circ$  does not change the dielectric properties of wood materials (Pozar 2011). So, when  $\mathbf{E}$  is arbitrarily oriented in space and forms an angle  $\theta_1$  with the longitudinal direction, angle  $\theta_2$  with the transversal direction, and angle  $\theta_3$  with the tangential direction, closed-form expressions for calculating the relative dielectric constant,  $\epsilon'$ , and the dielectric loss tangent,  $\tan \delta$ , is given in (Peyskens et al. 1984).

## 5 Enthalpy Model for Heating of Orthotropic Media

In anisotropic materials, thermal energy flows at different rates along different directions. This is taken into account by assigning a second-order tensor character to the thermal conductivity. The  $x$ -component of the heat flux vector  $q_x$  becomes (Bergman et al. 2011):

$$q_x = - \left( k_{xx} \frac{\partial T}{\partial x} + k_{xy} \frac{\partial T}{\partial y} + k_{xz} \frac{\partial T}{\partial z} \right) \tag{4}$$

and similarly for the other two directions. For orthotropic materials, heat still travels at different rates along different directions but the heat flux along any direction is driven only by the temperature gradient along that direction, i.e.  $k_{ij} = 0$  when  $i \neq j$ . The heat equation then becomes

$$\rho C_p \frac{\partial T}{\partial t} = \frac{\partial}{\partial x} \left( k_{xx}(T) \frac{\partial T}{\partial x} \right) + \frac{\partial}{\partial y} \left( k_{yy}(T) \frac{\partial T}{\partial y} \right) + \frac{\partial}{\partial z} \left( k_{zz}(T) \frac{\partial T}{\partial z} \right) \tag{5}$$

In this paper, we solve the energy equation in terms of the enthalpy function and assume that the interface  $\Gamma$  between the solid ( $\Omega^-$ ) and liquid ( $\Omega^+$ ) phases can be described by a regular function  $F(x, y, z, t) = 0$  (Hu and Argyropoulos 1995a, b). The temperature in the solid and liquid phases is denoted by  $T_s$  and  $T_l$  respectively. Using a temperature-based formulation, the two energy equations that govern both solid and liquid media are written in the absence of convective motion:

$$\begin{aligned} & \rho^s(T_s)C_p^s(T_s)\frac{\partial T_s}{\partial t} \\ &= \frac{\partial}{\partial x}\left(k_{xx}^s\frac{\partial T_s}{\partial x}\right) + \frac{\partial}{\partial y}\left(k_{yy}^s\frac{\partial T_s}{\partial y}\right) + \frac{\partial}{\partial z}\left(k_{zz}^s\frac{\partial T_s}{\partial z}\right), \quad F(x, y, z, t) < 0 \quad (6) \end{aligned}$$

$$\begin{aligned} & \rho^l(T_l)C_p^l(T_l)\frac{\partial T_l}{\partial t} \\ &= \frac{\partial}{\partial x}\left(k_{xx}^l\frac{\partial T_l}{\partial x}\right) + \frac{\partial}{\partial y}\left(k_{yy}^l\frac{\partial T_l}{\partial y}\right) + \frac{\partial}{\partial z}\left(k_{zz}^l\frac{\partial T_l}{\partial z}\right), \quad F(x, y, z, t) > 0 \quad (7) \end{aligned}$$

where  $\rho^s$  [kg/m<sup>3</sup>],  $C_p^s$  [J/kg/°C] and  $k^s$  [W/m/°C] are respectively the density, the specific heat capacity and the thermal conductivity of the material in the solid state.  $\rho^l$  [kg/m<sup>3</sup>],  $C_p^l$  [J/kg/°C] and  $k^l$  [W/m/°C] are respectively the density, specific heat capacity and thermal conductivity of the material in the liquid state.

The boundary conditions, also known as the Stefan conditions (Hu and Argyropoulos 1995a, b), allow us to consider the energy jump between the two phases:

$$T_s(x, y, z, t) = T_l(x, y, z, t); F(x, y, z, t) = 0 \quad (8)$$

$$\begin{aligned} & \left(k_x^s(T_s)\frac{\partial T_s}{\partial x}, k_y^s(T_s)\frac{\partial T_s}{\partial y}, k_z^s(T_s)\frac{\partial T_s}{\partial z}\right) \cdot \nabla F - \left(k_x^l(T_l)\frac{\partial T_l}{\partial x}, k_y^l(T_l)\frac{\partial T_l}{\partial y}, k_z^l(T_l)\frac{\partial T_l}{\partial z}\right) \cdot \nabla F \\ &= -\rho \cdot L \frac{\partial F}{\partial t} \quad (9) \end{aligned}$$

$L$  is the latent heat [J/kg].

In order to avoid numerical problems in the phase transition region, the variables were changed. The temperature-dependent density  $\rho(T)$  and specific heat capacity  $C_p(T)$  can be replaced by the volumetric specific enthalpy  $H(T)$  defined by (Nedjar 2002):

$$H(T) = \int_{T_{ref}}^T \rho(T)c_p(T)dT \quad (10)$$

where  $T_{ref}$  [°C] is a reference temperature.

The advantage of using an enthalpy—rather than a temperature-based formulation is that it simultaneously eliminates the doubling of the energy equation and the Stefan conditions. By introducing the volumetric specific enthalpy  $H(T)$  at the phase transition, the abrupt jump in the volumetric heat capacity is transformed into a relatively smoother temperature-dependent function. It can be shown that, around phase transition, the curvature of volumetric specific enthalpy  $H(T)$  is similar to that of thermal conductivity  $k(T)$ .  $H(T)$  depends strongly on the type of material, although a clear distinction must be made between the following two situations. In the first case, the phase change occurs in an interval  $[T_1^s - T_2^f]$ . In this case the enthalpy is



defined by:

$$H(T \leq T_1^s) = \int_{T_{ref}}^T \rho^s(T)C_p^s(T)dT \tag{11}$$

$$H(T_1^s < T \leq T_2^f) = \int_{T_{ref}}^{T_1^s} \rho^s(T)C_p^s(T)dT + \int_{T_1^s}^T \rho(T) \frac{\partial L}{\partial T} dT, \tag{12}$$

$$H(T > T_2^f) = \int_{T_{ref}}^{T_1^s} \rho^s(T)C_p^s(T)dT + \rho(T)L + \int_{T_2^f}^T \rho^f(T).C_p^f(T)dT \tag{13}$$

In the second case, the phase change occurs at a constant temperature so the enthalpy exhibits discontinuity at the fusion temperature,  $T_m (= T_1^s = T_2^f)$ , and is defined as follows:

$$H(T \leq T_m) = \int_{T_{ref}}^T \rho^s(T)C_p^s(T)dT \tag{14}$$

$$H(T > T_m) = \int_{T_{ref}}^{T_m} \rho^s(T)C_p^s(T)dT + \rho(T)L + \int_{T_m}^T \rho^f(T).C_p^f(T)dT \tag{15}$$

Zero enthalpy is defined at the saturated solid temperature. For purposes of numerical simulation, the enthalpy method is more reliable. However, the problem remains difficult and highly nonlinear. Following a procedure similar to the enthalpy transform method, the temperature-dependent thermal conductivity can be substituted by the thermal conductivity integral, using Kirchhoff’s transformation:

$$\begin{aligned} \theta_x(T \leq T_m) &= \int_{T_{ref}}^T k_{xx}^s(T)dT; \\ \theta_y(T \leq T_m) &= \int_{T_{ref}}^T k_{yy}^s(T)dT; \\ \theta_z(T \leq T_m) &= \int_{T_{ref}}^T k_{zz}^s(T)dT; \quad \forall T \end{aligned} \tag{16}$$

$$\begin{aligned}
 \theta_x(T > T_m) &= \int_{T_m}^T k_{xx}^l(T) dT; \\
 \theta_y(T > T_m) &= \int_{T_m}^T k_{yy}^l(T) dT; \\
 \theta_z(T > T_m) &= \int_{T_m}^T k_{zz}^l(T) dT
 \end{aligned}
 \tag{17}$$

To do so, we consider Leibniz’s rule (Flanders 1973) for differentiation under the integral sign in Eqs. (14)–(15) and (16)–(17):

$$\frac{\partial H}{\partial t} = \rho(T)c_p(T) \frac{\partial T}{\partial t}
 \tag{18}$$

$$\frac{\partial \theta_x}{\partial x} = k_{xx}(T) \frac{\partial T}{\partial x}; \quad \frac{\partial \theta_y}{\partial y} = k_{yy}(T) \frac{\partial T}{\partial y}; \quad \frac{\partial \theta_z}{\partial z} = k_{zz}(T) \frac{\partial T}{\partial z}
 \tag{19}$$

With these transformations, and taking into account the internal volumetric heat generation of microwave energy  $P_{wave}$ , the governing heat equation reduces to a partial differential system, with two mutually related dependent variables  $H$  and  $\theta = (\theta_x, \theta_y, \theta_z)$ :

$$\frac{\partial H(T)}{\partial T} = \left( \frac{\partial^2 \theta_x}{\partial x^2} + \frac{\partial^2 \theta_y}{\partial y^2} + \frac{\partial^2 \theta_z}{\partial z^2} \right) + P_{wave}
 \tag{20}$$

For microwaves sources, the internal volumetric heat generation of microwave energy  $P_{wave}$  is given by the following expression

$$P_{wave}(T) = -Re(\nabla \cdot S)
 \tag{21}$$

where  $S$  is the instantaneous Poynting vector. To solve the problem, we introduce the boundary condition into Eq. (22) as follows:

$$\left( n_x \frac{\partial \theta_x}{\partial x} + n_y \frac{\partial \theta_y}{\partial y} + n_z \frac{\partial \theta_z}{\partial z} \right) + h(T - T_\infty) - \mathbf{q} \cdot \mathbf{n} = 0
 \tag{22}$$

where  $\mathbf{q}$  [W/m<sup>2</sup>] is the radiative heat flux incident,  $\mathbf{n}$  is the outward normal ( $n_x, n_y, n_z$ ) to the surface  $h$ , [W/m<sup>2</sup>/°C] is the surface heat transfer coefficient, and  $T_\infty$  is the temperature of the surrounding medium (air). The term  $h(T - T_\infty)$  represents the convection heat transfer from the material to the environment. The incident heat flux depends on the source configuration and the position of the material. The advantage

of using an enthalpy- rather than a temperature-based formulation is that it simultaneously eliminates the doubling of the energy equation and the Stefan conditions (Erchiqui 2013a, b).

### 5.1 Implicit Time Integration Scheme

Numerical time approximation schemes are used mainly to obtain the transient response. These numerical integration schemes derive recursion relations that relate  $H(t)$  at a moment of time  $t$  to  $H(t + \Delta t)$  at another moment of time  $t + \Delta t$ . The solution is then solved step by step starting from the initial conditions at time  $t = 0$  until the desired duration of the transient response is calculated. The most common numerical schemes for the solution of Eq. (20) belong to the weighted Euler difference family of time approximations, as follows (Dokainish and Subbraj 1989):

$$H^{n+\theta} = (1 - \theta)H^n + \theta H^{n+1}, \text{ with } \theta = \frac{t - t_n}{\Delta t} \tag{23}$$

The parameter  $\theta$  varies in the range  $[0-1]$ . The  $\theta$  schemes are unconditionally stable when  $\theta \leq 1/2$  and  $O(\Delta t)$  are accurate, with the exception of the  $O(\Delta t^2)$ -convergent Crank–Nicolson scheme ( $\theta = 1/2$ ). Setting  $\theta = 1$  leads to the backward Euler (fully implicit) scheme, which is only first-order accurate but very stable and hence ideally suited for integration. In the present study, we consistently use the semi-implicit Crank–Nicolson scheme (Dokainish and Subbraj 1989). In this case, Eq. (24) becomes:

$$(K_{n+1}^* + G_{n+1}^*)H_{n+1} = K_n^*H_n + G_n^*H_n^2 + R_{n,n+1}^* \tag{24}$$

where  $K^*$ ,  $G^*$  and  $R^*$  are modified global matrices and  $H_{n+1}$  is the vector of global nodal enthalpies at moment  $t_{n+1}$ .

## 6 Electromagnetic-Wave Energy and Poynting’s Theorem

The time-dependent power flow density of an electromagnetic wave is given by the instantaneous Poynting vector  $S$  (Poazar 2011):

$$S = \frac{1}{2}E \times H^* \tag{25}$$

$E$  and  $H^*$  are the electric field ( $V\ m^{-1}$ ) and the conjugate magnetic field intensity ( $A\ m^{-1}$ ), respectively. In general, we are dealing with steady-state harmonic time-varying fields. It is convenient to represent each field vector as a complex phasor by

applying a Fourier transform. Assuming that we have a monochromatic wave, we can write:

$$\mathbf{E}(\mathbf{r}, t) = e^{-j\omega t} \overline{\mathbf{E}}(\mathbf{r}) \quad (26)$$

where  $\overline{\mathbf{E}}$  is a complex vector and a function of  $\mathbf{r}$  (m), and  $\omega$  (radian  $s^{-1}$ ) is the angular frequency of the incident radiation. The other field vectors can be written using the same notation as in Eq. (26).

### 6.1 Maxwell's Equations and Power Dissipation

A propagating electromagnetic wave is composed of oscillating electric ( $\mathbf{E}$ ) and magnetic ( $\mathbf{H}$ ) fields. The space and time dependence of these fields are described by the following Maxwell's equations:

$$\nabla \times \mathbf{E} = -\frac{\partial \mathbf{B}}{\partial t}, \quad (27)$$

$$\nabla \times \mathbf{H} = \mathbf{J} - \frac{\partial \mathbf{D}}{\partial t}, \quad (28)$$

where  $\mathbf{E}$ ,  $\mathbf{B}$ ,  $\mathbf{H}$ ,  $\mathbf{J}$  and  $\mathbf{D}$  are the electric field ( $V m^{-1}$ ), the magnetic field ( $Wb m^{-2}$ ), the magnetic induction ( $A m^{-1}$ ), the current density ( $A m^{-2}$ ), and the electric displacement ( $C m^{-2}$ ), respectively.

Considering the definition of the Poynting vector  $\mathbf{S}$ , as in (25), and using both the identity vector and Maxwell's equations with the complex conjugate field  $\mathbf{H}$ , (29) can be derived from (27) and (28) as follows:

$$\begin{aligned} \nabla \cdot \mathbf{S} &= \frac{1}{2} \nabla \cdot (\mathbf{E} \times \mathbf{H}^*) = -\frac{1}{2} [\mathbf{E} \cdot (\nabla \times \mathbf{H}^*) - \mathbf{H}^* \cdot (\nabla \times \mathbf{E})] \\ &= -\frac{1}{2} \left( \mathbf{E} \cdot \frac{\partial \mathbf{D}^*}{\partial t} + \mathbf{E} \cdot \mathbf{J}^* + \mathbf{H}^* \cdot \frac{\partial \mathbf{B}}{\partial t} \right) \end{aligned} \quad (29)$$

The vector  $\mathbf{S}$  depends on the explicit electric currents, the temporal variations of the electric displacement, and the magnetic induction.

### 6.2 The Case of Anisotropic Dielectric Materials

For anisotropic dielectric wood, both the electric charge density ( $\rho$ ) and the electric currents ( $\mathbf{J}$ ) are equal to zero. Furthermore, the following linear interrelations can be established between the electric and magnetic properties:

$$\mathbf{D} = \varepsilon_0 \bar{\bar{\boldsymbol{\varepsilon}}} \cdot \mathbf{E} \quad (30)$$

$$\mathbf{B} = \mu_0 \bar{\bar{\boldsymbol{\mu}}} \cdot \mathbf{H} \quad (31)$$

$$\mathbf{J} = 0 \quad (32)$$

where  $\varepsilon_0$  is the dielectric permittivity ( $= 8.8541 \times 10^{-12}$  F/m) of the free space and  $\mu_0$  is the permeability of vacuum ( $= 4\pi \times 10^{-7} \cong \text{H/m}$ ).  $\bar{\bar{\boldsymbol{\varepsilon}}}$  and  $\bar{\bar{\boldsymbol{\mu}}}$  are, respectively, the relative dielectric and permeability tensors:

$$\bar{\bar{\boldsymbol{\varepsilon}}} = \text{Re}(\bar{\bar{\boldsymbol{\varepsilon}}}) - j\text{Im}(\bar{\bar{\boldsymbol{\varepsilon}}}) \text{ and } \bar{\bar{\boldsymbol{\mu}}} = \text{Re}(\bar{\bar{\boldsymbol{\mu}}}) - j\text{Im}(\bar{\bar{\boldsymbol{\mu}}}) \quad (33)$$

with:

$$\text{Re}(\bar{\bar{\boldsymbol{\varepsilon}}}) = \begin{bmatrix} \varepsilon'_{LL} & \varepsilon'_{LR} & \varepsilon'_{LT} \\ \varepsilon'_{RL} & \varepsilon'_{RR} & \varepsilon'_{RT} \\ \varepsilon'_{TL} & \varepsilon'_{TR} & \varepsilon'_{TT} \end{bmatrix}, \quad \text{Im}(\bar{\bar{\boldsymbol{\varepsilon}}}) = \begin{bmatrix} \varepsilon''_{LL} & \varepsilon''_{LR} & \varepsilon''_{LT} \\ \varepsilon''_{RL} & \varepsilon''_{RR} & \varepsilon''_{RT} \\ \varepsilon''_{TL} & \varepsilon''_{TR} & \varepsilon''_{TT} \end{bmatrix} \quad (34)$$

and

$$\text{Re}(\bar{\bar{\boldsymbol{\mu}}}) = \begin{bmatrix} \mu'_{LL} & \mu'_{LR} & \mu'_{LT} \\ \mu'_{RL} & \mu'_{RR} & \mu'_{RT} \\ \mu'_{TL} & \mu'_{TR} & \mu'_{TT} \end{bmatrix}, \quad \text{Im}(\bar{\bar{\boldsymbol{\mu}}}) = \begin{bmatrix} \mu''_{LL} & \mu''_{LR} & \mu''_{LT} \\ \mu''_{RL} & \mu''_{RR} & \mu''_{RT} \\ \mu''_{TL} & \mu''_{TR} & \mu''_{TT} \end{bmatrix} \quad (35)$$

The subscripts L, R, and T are respectively the longitudinal, radial, and tangential directions.

In general, we are dealing here with steady-state harmonic time-varying fields. It is convenient to represent each field vector as a complex phasor by applying a Fourier transform. Assuming that we have a monochromatic wave, we can write:

$$\mathbf{E}(\mathbf{r}, t) = e^{-j\omega t} \bar{\mathbf{E}}(\mathbf{r}), \quad (36)$$

where  $\bar{\mathbf{E}}$  is a complex vector and function of  $\mathbf{r}$ , and  $\omega$  is the angular frequency of the wave. The other field vectors can be written using the same notation of Eq. (36).

Following the application of (30)–(32) and (36), (29) will be reduced to the equation below:

$$\nabla \cdot \mathbf{S} = -j \frac{\omega}{2} \left( \left[ \varepsilon_0 (\bar{\mathbf{E}} \cdot \bar{\boldsymbol{\varepsilon}} \cdot \bar{\mathbf{E}}^*) \right] + \left[ \mu_0 (\bar{\mathbf{H}} \cdot \bar{\boldsymbol{\mu}} \cdot \bar{\mathbf{H}}^*) \right] \right) \quad (37)$$

Introducing the complex expressions of the dielectric permittivity and the magnetic permeability tensors, we get from (37):

$$\text{Re}(\nabla \cdot \mathbf{S}) = -\frac{\omega}{2} \left( \varepsilon_0 (\bar{\mathbf{E}} \cdot \text{Im}(\bar{\boldsymbol{\varepsilon}}) \cdot \bar{\mathbf{E}}^*) + \mu_0 (\bar{\mathbf{H}} \cdot \text{Im}(\bar{\boldsymbol{\mu}}) \cdot \bar{\mathbf{H}}^*) \right) \quad (38)$$

$$\text{Im}(\nabla \cdot \mathbf{S}) = -2\omega \left( \frac{1}{4} \varepsilon_0 (\bar{\mathbf{E}} \cdot \text{Re}(\bar{\boldsymbol{\varepsilon}}) \cdot \bar{\mathbf{E}}^*) + \frac{1}{4} \mu_0 (\bar{\mathbf{H}} \cdot \text{Re}(\bar{\boldsymbol{\mu}}) \cdot \bar{\mathbf{H}}^*) \right) \quad (39)$$

Note that (38) shows that the real part of  $(\nabla \cdot \mathbf{S})$  is equal to the power dissipated per unit volume in the form of heat. The imaginary part of the complex  $(\nabla \cdot \mathbf{S})$ , Eq. (39), is equal to  $2\omega$  times the net reactive power stored per unit volume and time-average of electric  $W_e$  and magnetic  $W_m$  energy densities (Hollis 1983):

$$\langle W_e \rangle = \text{Im} \left( \frac{1}{T} \int_0^T W_e dt \right) = \frac{1}{4} \varepsilon_0 (\bar{\mathbf{E}} \cdot \text{Re}(\bar{\boldsymbol{\varepsilon}}) \cdot \bar{\mathbf{E}}^*) \quad (40)$$

$$\langle W_m \rangle = \text{Im} \left( \frac{1}{T} \int_0^T W_m dt \right) = \frac{1}{4} \mu_0 (\bar{\mathbf{H}} \cdot \text{Re}(\bar{\boldsymbol{\mu}}) \cdot \bar{\mathbf{H}}^*) \quad (41)$$

where  $W_e$  and  $W_m$  are respectively the instantaneous electric and magnetic energy densities, and  $T$  is the period. The quantity  $(\langle W_e \rangle + \langle W_m \rangle)$  ( $\text{J}/\text{m}^3$ ) is the total time average stored energy density of the electromagnetic field in the anisotropic dielectric material.

The real part of the complex  $(\nabla \cdot \mathbf{S})$ , is equal to  $2\omega$  times the net power dissipated per unit volume and time-average of electric  $\langle W_e \rangle$  and magnetic  $\langle W_m \rangle$  energy densities:

$$P_{wave} = \frac{\omega}{2} \left( \varepsilon_0 (\bar{\mathbf{E}} \cdot \text{Im}(\bar{\boldsymbol{\varepsilon}}) \cdot \bar{\mathbf{E}}^*) + \mu_0 (\bar{\mathbf{H}} \cdot \text{Im}(\bar{\boldsymbol{\mu}}) \cdot \bar{\mathbf{H}}^*) \right) \quad (42)$$

$\varepsilon_0$  is the dielectric permittivity ( $= 8.8541 \times 10^{-12}$  F/m) of the free space and  $\mu_0$  is the permeability of vacuum ( $= 4\pi \times 10^{-7} \cong \mathbf{H}/\text{m}$ ).  $\bar{\boldsymbol{\varepsilon}}$  and  $\bar{\boldsymbol{\mu}}$  are, respectively, the complex relative dielectric and complex permeability tensors. In wood systems, the magnetic permeability tensor  $\bar{\boldsymbol{\mu}}$  is closely approximated by the real tensor  $\mu_0 \bar{\mathbf{I}}$ ; ( $\bar{\mathbf{I}}$  is the identity tensor), (Kaestner and Bååth 2005). This is what we assumed in this paper. Thus, the power dissipated per unit volume, as in (42), becomes:

$$P_{wave} = \frac{\omega}{2} \varepsilon_0 (\mathbf{E} \cdot \text{Im}(\bar{\boldsymbol{\varepsilon}}) \cdot \mathbf{E}) \quad (43)$$

Computing the power dissipation involves determining the electric field as a function of the position within the material. If  $\mathbf{E}$  is parallel with one of the three principal directions (longitudinal, radial or tangential) of the wood sample, the power dissipated per unit volume may be simplified as (see Appendix):

$$P_{net} = \frac{\omega}{2} \varepsilon_0 \varepsilon_d'' E_d^2 \quad (44)$$

where  $\varepsilon_d''$  is the dielectric constant in the principal direction  $d$ : longitudinal (L), radial (R) and tangential (T). Assuming the electro-neutrality of wood ( $\nabla(\nabla \cdot \mathbf{E}) = 0$ ), we

deduce for each principal direction from Maxwell's equations the expression of Helmholtz's equation of wave propagation (Erchiqui 2013a, b):

$$\nabla^2 \bar{\mathbf{E}} - \gamma^2 \bar{\mathbf{E}} = 0 \tag{45}$$

where  $\gamma$  is the constant complex propagation  $\gamma = \alpha + j\beta$ ,  $\beta$  is the attenuation constant and  $\alpha$  is the phase (a constant). These parameters are related to the dielectric properties of the material and frequency of radiation by:

$$\alpha = \frac{\omega}{c} \sqrt{\frac{\epsilon'}{2} (\sqrt{1 + \tan^2 \delta} + 1)} \quad \beta = \frac{\omega}{c} \sqrt{\frac{\epsilon'}{2} (\sqrt{1 + \tan^2 \delta} - 1)} \tag{46}$$

$c = 1/\sqrt{\mu_0 \epsilon_0}$  is the speed of light. The term  $\delta (= \text{tg}^{-1}(\epsilon''/\epsilon'))$  is the dielectric loss angle. The attenuation constant,  $\beta$ , controls the rate at which the incident field intensity decays into a sample.  $1/(2\beta)$  is known as the penetration depth (d). The phase constant,  $\alpha$ , represents the change of phase of the propagation radiation and is related to the wavelength of radiation by  $\lambda = 2\pi/\alpha$ .

### 6.3 Uniform Plane Wave Propagation and Power Dissipation

In this paper, we assume that each component of the electric field  $\mathbf{E} = (\mathbf{E}_x, \mathbf{E}_y, \mathbf{E}_z)$  is a uniform plane microwave. Also, each component of a wave is assumed to be incident normally on opposite faces of the sample:

x direction: longitudinal direction L

$$\mathbf{E}_x = E_x(z) \mathbf{a}_x \tag{47}$$

y direction: radial direction R

$$\mathbf{E}_y = E_y(x) \mathbf{a}_y \tag{48}$$

z direction: tangential direction T

$$\mathbf{E}_z = E_z(y) \mathbf{a}_z \tag{49}$$

where x is a component of the electric field ( $E_x$ ), which is a function of the parameter z, y is a component of the electric field ( $E_y$ ), which is a function of the parameter x, and z is a component of the electric field ( $E_z$ ), which is a function of the parameter y (see Fig. 2).

For each direction, according to Eq. (45), we have the following expression for Helmholtz's equation of wave propagation:

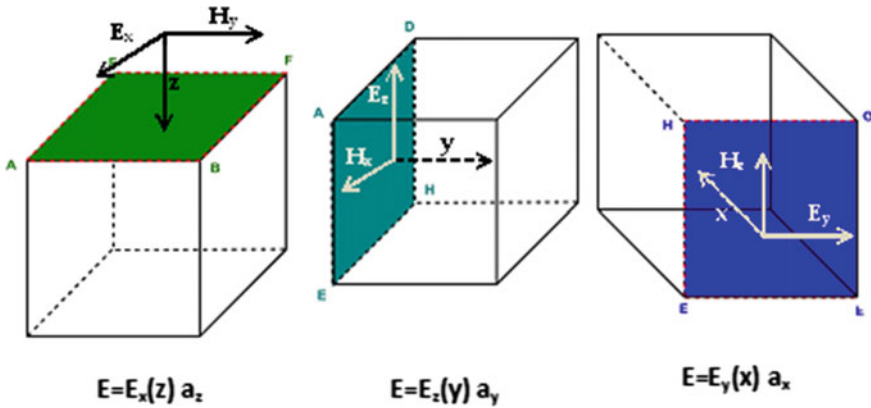


Fig. 2 Schematic of sample wood exposed to plane microwaves from the three principal faces

Longitudinal direction:

$$\frac{d^2 E_z}{dy^2} \mathbf{a}_z - \gamma_y^2 E_z \mathbf{a}_z = 0, \quad 0 \leq y \leq L_y \tag{50}$$

Radial direction:

$$\frac{d^2 E_y}{dx^2} \mathbf{a}_y - \gamma_x^2 E_y \mathbf{a}_y = 0, \quad 0 \leq x \leq L_x \tag{51}$$

Tangential direction:

$$\frac{d^2 E_x}{dz^2} \mathbf{a}_x - \gamma_z^2 E_x \mathbf{a}_x = 0, \quad 0 \leq z \leq L_z \tag{52}$$

$L_x$ ,  $L_y$  and  $L_z$  are, respectively, the length of the sample wood in the  $x$ ,  $y$  and  $z$  directions (see Fig. 1). The unit vectors  $\mathbf{a}_z$ ,  $\mathbf{a}_y$  and  $\mathbf{a}_x$  are, respectively, the normal to the surface (AEFB), (ADHE) and (HCTE) of the sample wood (see Fig. 2).

The waves travel through the material from right to left with an incident power flux  $I_0$ . The regions external to the sample are denoted by index 1 for the left and index 3 for the right. The material is denoted by index 2. The exact solutions for the power absorbed of each principal direction of material are given respectively by the following expressions (Erchiqui 2013a, b):

Longitudinal direction:

$$P_{wave}^x = 2I_0^x \beta^x \left[ \frac{e^{-2\beta^x x} + (\bar{R}_{23}^x)^2 e^{-4\beta^x L_x} e^{2\beta^x x} + 2\bar{R}_{23}^x e^{-2\beta^x L_x} \cos(2\alpha^x(x - L_x) - \frac{x}{23})}{1 + (\bar{R}_{12}^x)^2 (\bar{R}_{23}^x)^2 e^{-4\beta^x L_x} - 2\bar{R}_{12}^x \bar{R}_{23}^x \cos(\frac{x}{12} + \frac{x}{23} + 2\alpha^x L_x)} e^{-2\beta^x L_x} \right] \tag{53}$$



Radial direction:

$$P_{wave}^y = 2I_0^y \beta^y \left[ \frac{e^{-2\beta^y y} + (\bar{R}_{23}^y)^2 e^{-4\beta^x L_y} e^{2\beta^y y} + 2\bar{R}_{23}^y e^{-2\beta^y L_y} \cos(2\alpha^y (y - L_y) - \frac{y}{23})}{1 + (\bar{R}_{12}^y)^2 (\bar{R}_{23}^y)^2 e^{-4\beta^y L_y} - 2\bar{R}_{12}^y \bar{R}_{23}^y \cos(\frac{y}{12} + \frac{y}{23} + 2\alpha^y L_y)} e^{-2\beta^y L_y} \right] \quad (54)$$

Tangential direction:

$$P_{wave}^z = 2I_0^z \beta^z \left[ \frac{e^{-2\beta^z z} + (\bar{R}_{23}^z)^2 e^{-4\beta^z L_z} e^{2\beta^z z} + 2\bar{R}_{23}^z e^{-2\beta^z L_z} \cos(2\alpha^z (z - L_z) - \frac{z}{23})}{1 + (\bar{R}_{12}^z)^2 (\bar{R}_{23}^z)^2 e^{-4\beta^z L_z} - 2\bar{R}_{12}^z \bar{R}_{23}^z \cos(\frac{z}{12} + \frac{z}{23} + 2\alpha^z L_z)} e^{-2\beta^z L_z} \right] \quad (55)$$

The superscripts x, y, z are associated respectively with the longitudinal, radial and tangential directions.  $\theta_{ij}$  is the phase angle for reflection coefficient at the interface between layers i and j.  $\bar{R}_{ij}$  is the absolute value of the complex reflection coefficient.

## 7 Validation of the Proposed Method

To validate the proposed approach, three situations are considered: (i) heat transfer in one-dimensional raw beef sample exposed to microwave energy (Ayappa et al. 1991), (ii) heat transfer in an orthotropic plate with imposed temperatures (Bruch and Zyrolowski 1974) and (iii) heat transfer of frozen wood with phase change: imposed temperatures (Steinhagen and Harry 1988).

### 7.1 Numerical Heating Validation

To validate the specific volumetric enthalpy-based finite element developed in this work, we consider the results obtained in for a raw beef sample exposed to microwave radiation. In this example, the author solves an isothermal heat conduction equation where the dielectric and thermophysical properties are constants. For our study, we consider a linear mesh with 42 elements and 41 nodes. Figure 3 compares the power distribution and the predicted temperature profile for the raw beef sample exposed to radiation from the left face. The results obtained in (Ayappa et al. 1991) are similar to ours for both formulations.

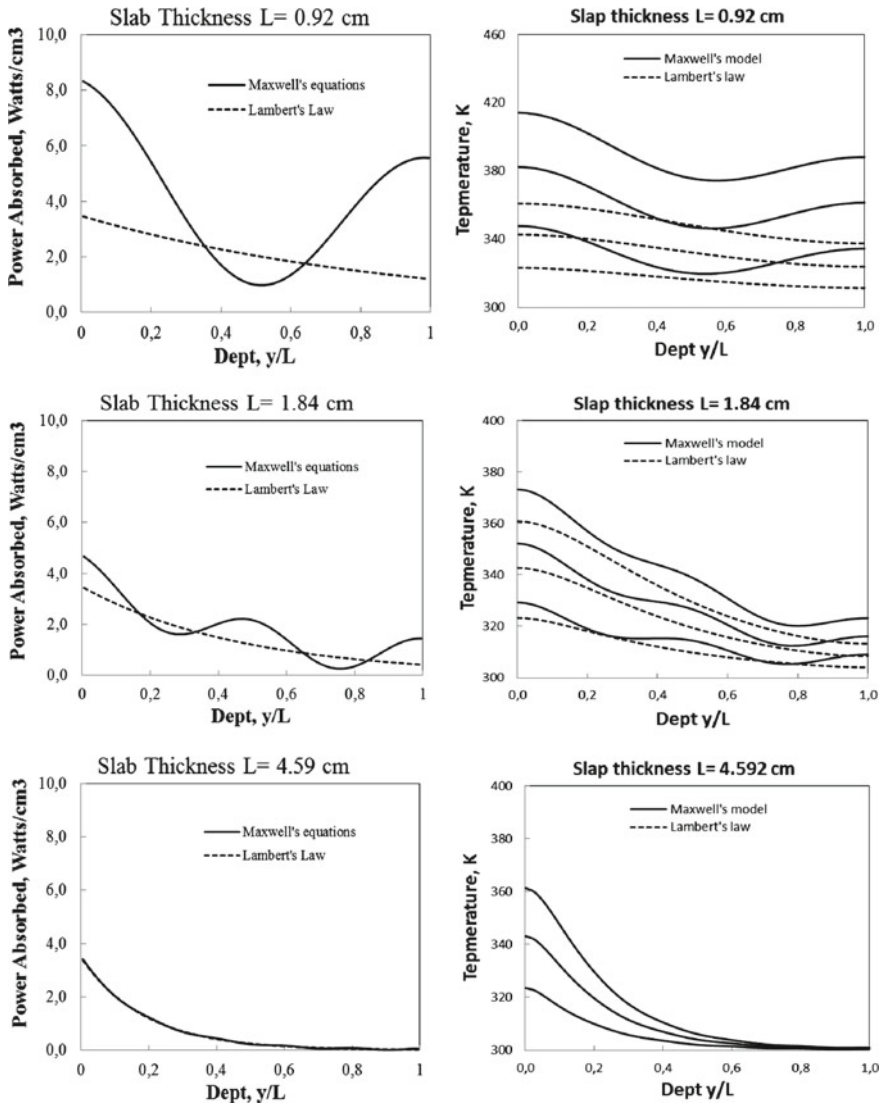


Fig. 3 Influence of slab thickness on power and predicted temperature for raw beef sample exposed to microwave from the left,  $I_0 = 3 \text{ W/cm}^2$ ,  $f = 2450 \text{ MHz}$

### 7.2 Analytical Heat Transfer in an Orthotropic Plate: Imposed Temperatures

For analytical validation, we consider an orthotropic plate subjected to a uniform temperature. The temperature  $T(x, y, t)$  across the thickness with time  $t$  is computed

**Table 1** Geometrical and thermophysical properties of material

Density $\rho$ (kg/m <sup>3</sup> )	1.0
Specific heat $C_p$ (J kg <sup>-1</sup> °C <sup>-1</sup> )	1.0
Thermal conductivity $k_x$ , x direction, (W m <sup>-1</sup> °C <sup>-1</sup> )	0.2
Thermal conductivity $k_y$ , y direction, (W m <sup>-1</sup> °C <sup>-1</sup> )	0.4
Length in x direction (m)	1.0
Length in y direction (m)	1.0

using Laplace transforms to solve the 2D energy equation with an imposed temperature (Bruch and Zyrolowski 1974). The thickness as well as the physical properties of material used in the numerical validation is given in Table 1. For the finite-element analysis, we consider a quadrilateral mesh with 400 elements and 441 nodes. In the case where the initial temperature of the plate is 30 °C and the imposed temperature is 0 °C, the analytical solution is given by the following equation (Bruch and Zyrolowski 1974):

$$T(x, y, t) = \sum_{n=1}^{\infty} \sum_{j=1}^{\infty} A_n \sin \frac{n\pi x}{L_x} \sin \frac{j\pi y}{L_y} \exp \left[ - \left( \frac{k_x n^2 \pi^2}{L_x^2} + \frac{k_y j^2 \pi^2}{L_y^2} \right) \frac{t}{\rho C_p} \right] \quad (56)$$

where:

$$A_n = \left[ \frac{120}{\pi^2 j n} [(-1)^n - 1] [(-1)^j - 1] \right] \quad (57)$$

where  $k_x$  and  $k_y$  are respectively the thermal conductivity in the x and y directions.  $L_x$  and  $L_y$  are respectively the length and width of the plate. Table 2 compares, at  $t = 0.25$  s, the predicted temperature obtained by the theoretical equation with the volumetric enthalpy based on the finite-element method. The results illustrate the excellent agreement between the theoretical and numerical solutions. The agreement is very good with an error of less than 1.0%. For greater precision, a more refined mesh is necessary.

### 7.3 Experimental Heating Validation: Transient Heating of Frozen Logs

In this section, firstly, we consider the experimental temperature measurements obtained for transient heating of frozen logs (Steinhagen and Harry 1988), then, those obtained in (Peralta and Bangi 2006). For both tests, it involves heating a tree trunk immersed in water at a temperature of 54 °C. In the first case, it is trembling aspen log (radius is 0.3175 m and its initial temperature is -22 °C). In the second

**Table 2** Temperature distribution at time = 0.25 s

Y (m)	X (m)					
	0.0	0.2	0.4	0.6	0.8	1.0
0.0	0.000 <sup>a</sup>	0.000 <sup>a</sup>	0.000 <sup>a</sup>	0.000 <sup>a</sup>	0.000 <sup>a</sup>	0.000 <sup>a</sup>
	0.000	0.000	0.000	0.000	0.000	0.000
0.2	0.000 <sup>a</sup>	3.832 <sup>a</sup>	6.196 <sup>a</sup>	6.196 <sup>a</sup>	3.832 <sup>a</sup>	0.000 <sup>a</sup>
	0.000	3.864	6.250	6.250	3.864	0.000
0.4	0.000 <sup>a</sup>	6.121 <sup>a</sup>	9.898 <sup>a</sup>	9.898 <sup>a</sup>	6.121 <sup>a</sup>	0.000 <sup>a</sup>
	0.000	6.163	9.969	9.969	6.163	0.000
0.6	0.000 <sup>a</sup>	6.121 <sup>a</sup>	9.898 <sup>a</sup>	9.898 <sup>a</sup>	6.121 <sup>a</sup>	0.000 <sup>a</sup>
	0.000	6.163	9.969	9.969	6.163	0.000
0.8	0.000 <sup>a</sup>	3.832 <sup>a</sup>	6.196 <sup>a</sup>	6.196 <sup>a</sup>	3.832 <sup>a</sup>	0.000 <sup>a</sup>
	0.000	3.864	6.250	6.250	3.864	0.000
1.0	0.000 <sup>a</sup>	0.000 <sup>a</sup>	0.000 <sup>a</sup>	0.000 <sup>a</sup>	0.000 <sup>a</sup>	0.000 <sup>a</sup>
	0.000	0.000	0.000	0.000	0.000	0.000

<sup>a</sup>Numerical results with *ThermoForm* code

test, it is eastern white pine log (the trunk radius is 0.2285 m and its initial temperature is  $-23\text{ }^{\circ}\text{C}$ ). In (Steinhagen and Harry 1988), it is assumed that logs is subjected to radial heating. In (Peralta and Bangi 2006), it is assumed that logs is subjected to orthotropic heating (radial and longitudinal). For both tests, the heating time is 60 h. The thermo-physical properties of the wood material are given in (Steinhagen and Harry 1988) and (Peralta and Bangi 2006) respectively. For finite element analysis, we consider a quadrilateral mesh (see Fig. 4).

In Fig. 5, we presented the history of the temperature obtained numerically and experimentally in the center of the trembling aspen trunk (Steinhagen and Harry

**Fig. 4** Circular (2D) geometry mesh

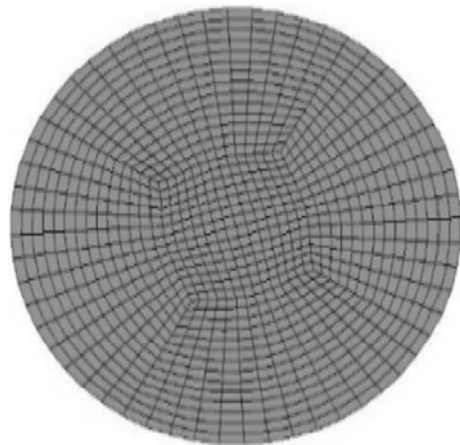
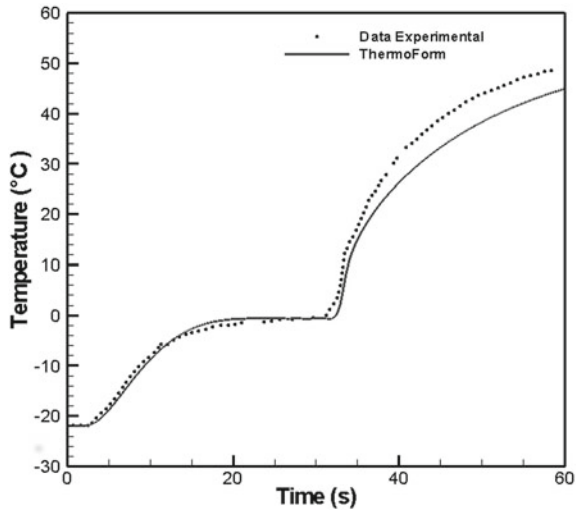


**Fig. 5** Experimental end numerical temperature versus heating time at the centre of log



1988). Figure 6 illustrates views of the numerical temperature distribution at different times: 900, 1800, 2700, and 3600 min.

In Fig. 7, we presented the temperature against heating time for three different points located 22.9 cm (location 1), 10.2 cm (location 2), and 2.5 cm (location 3) from the surface of an eastern white pine log (Peralta and Bangi 2006). The numerical results for the heating of frozen wood showed an excellent agreement with the experimental data, in both cases of tests.

## 8 Numerical Application: Characterization of the Time of Phytosanitary Treatment Wood by Microwaves

This study focused on 22-mm-thick boards. This dimension corresponds to the standard value for boards used in the manufacture of EUR EPAL® pallets. For this, a 3D wood log is considered for three wood species: *trembling aspen*, *white birch* and *sugar maple*. The log is considered to be orthotropic and its thermal and dielectric properties are functions of temperature, moisture content and structural orientation. The log structure is square ( $L_x = L_y = L_z = 2.2$  cm). The principal orientations in sample woods are indicated by x for the longitudinal direction (L), y for the radial direction (R), and z for the tangential direction (T).

To analyze the thermal and dielectric anisotropy effect on thawing frozen wood using microwave energy, we considered the following situation:

$$k_L = 1.8k_R \text{ and } k_T = 0.9k_R \tag{58}$$

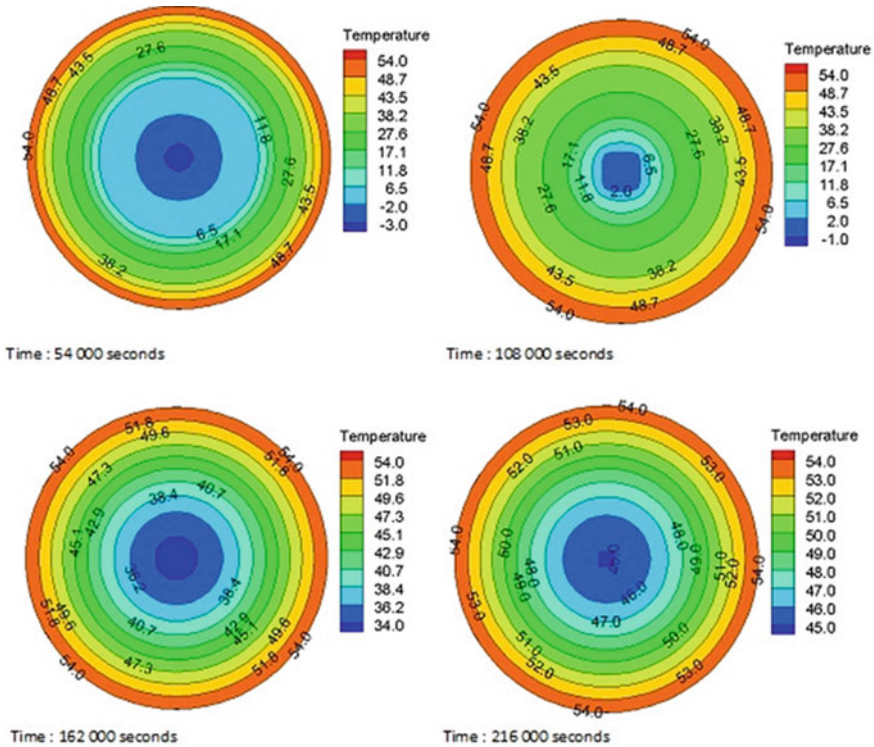
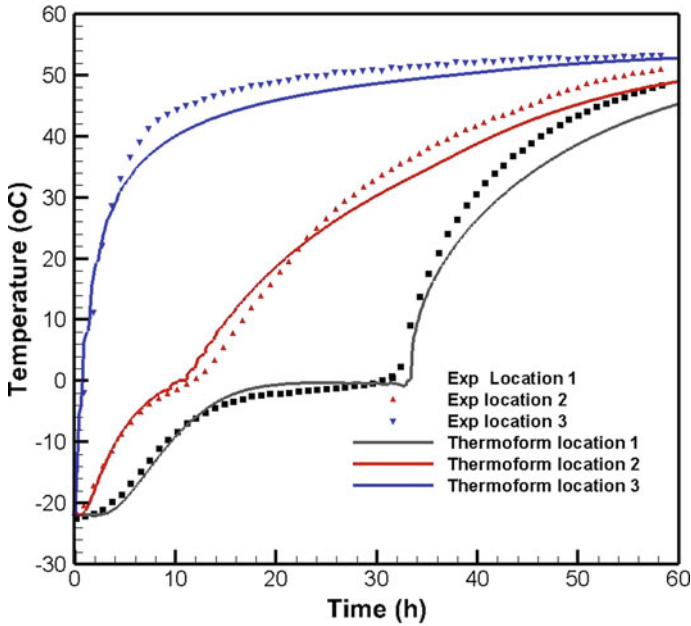


Fig. 6 Temperature versus heating time at the centre of log

$$\epsilon_L = 1.8\epsilon_R \text{ and } \epsilon_T = 0.9\epsilon_R \tag{59}$$

The wood material is exposed to radiation of equal intensity ( $1 \text{ W/cm}^2$ ) and frequency (2466 MHz from six faces): two faces in the x direction, two faces in the y direction, and two faces in the z direction. The initial wood temperature varies from  $-20$  to  $20 \text{ }^\circ\text{C}$ . The no-isothermal complex dielectric properties of the three wood species, for a moisture content (MC) at 131% (MC), are given in (Erchiqui et al. 2020). The specific gravity (SG) is 0.32, 0.48 and 0.55 for aspen, white birch and sugar maple respectively. The no-isothermal longitudinal relative dielectric constant  $\epsilon'$  and the relative dielectric loss  $\epsilon''$  are given in reference (Erchiqui et al. 2020). In this application, the density ( $\rho$ ), specific heat capacity ( $C_p$ ) and radial conductivity ( $k_R$ ) are calculated by the formulas provided in (Steinhagen and Harry 1988).

Figure 8 presents, at time 200 s and initial temperature  $-20 \text{ }^\circ\text{C}$ , different views of the surface temperature distribution induced by microwave treatment of the aspen trembling, birch white and sugar maple. At this time, Fig. 9 presents, for the trembling aspen log on the half-planes of symmetry (longitudinal, radial and tangential directions), the profiles of temperature distribution predicted from the power dissipation computed from Maxwell's equations.



**Fig. 7** Experimental and numerical temperature versus heating time for three different points located from the surface of an eastern white pine log

Figure 9(b–d) show different views of the temperature distribution in the longitudinal, radial and tangential directions, respectively. Similarly, Figs. 10 and 11 present the temperature distribution profiles for sugar maple and white birch, respectively. Significant differences can clearly be seen in temperature distribution when comparing the three directions and the three studied woods. In fact, for aspen and sugar maple, the longitudinal direction of the wood is preferred to temperature increase. On the other hand, for white birch, we note that the temperature profile associated with the longitudinal direction dominates at the edges and the center of the sample. Beyond these regions, for white birch, the temperature profile associated with the tangential direction dominates. One can also note that the highest temperatures were reached for the aspen wood sample, followed by white birch.

From the thermo-physical point of view, since the thermal conductivity and specific heat of each of the three hardwoods involve the same formulas, see reference (Steinhagen and Harry 1988), these differences could only be attributed to the differences in the density of these woods. As illustrated in Table 3, aspen is lighter while sugar is the densest wood. Indeed, the heating time increases with the density. This confirmation is due to the dependence of the volume enthalpy on density. In the melting zone (solid ice), the latent melting enthalpy of fusion is proportional to the density ( $\rho_L$ ). Also, from the electromagnetic point of view, the oscillatory nature of the electromagnetic wave is another parameter which affects the temperature profile. Indeed, the propagation of electromagnetic radiation in a wood medium is a result of



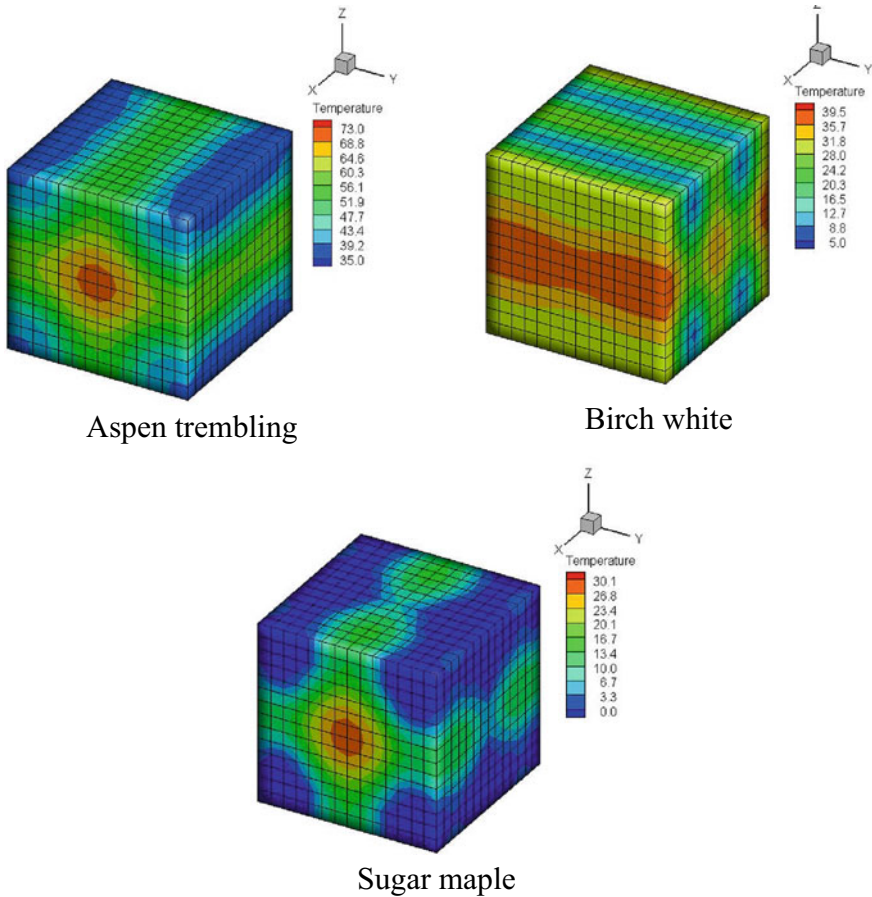


**Fig. 8** Surface temperature distribution for aspen trembling, white birch and sugar maple, exposed to microwave at time = 200 s,  $I_0 = 1 \text{ W/cm}^2$ ,  $f = 2466 \text{ MHz}$ ,  $T_0 = -20 \text{ }^\circ\text{C}$

a transmitted microwave at the incident face and a reflected microwave from the end surface. This situation, which affects the quality of the signal of the power absorbed by the wood, also affects the temperature profile. Indeed, a slight difference between the dielectric properties in the radial and tangential directions can have significant effects on the temperature profiles and power distributions. Consequently, it is very difficult to predict, from the complex dielectric and thermophysical properties of wood, the evolution of the temperature profile. Under these conditions, the experimental tools for characterization and the numerical modeling (mass transfer, phase change and thermomechanical and electromagnetic interactions) must be considered.

For the following analysis, we denote TA, WB and SM the trembling aspen, white birch and sugar maple. Figures 12, 13 and 14 represent the times required to eliminate 10, 25, 50, 75, and 100% of pathogens by microwave energy from trembling aspen,



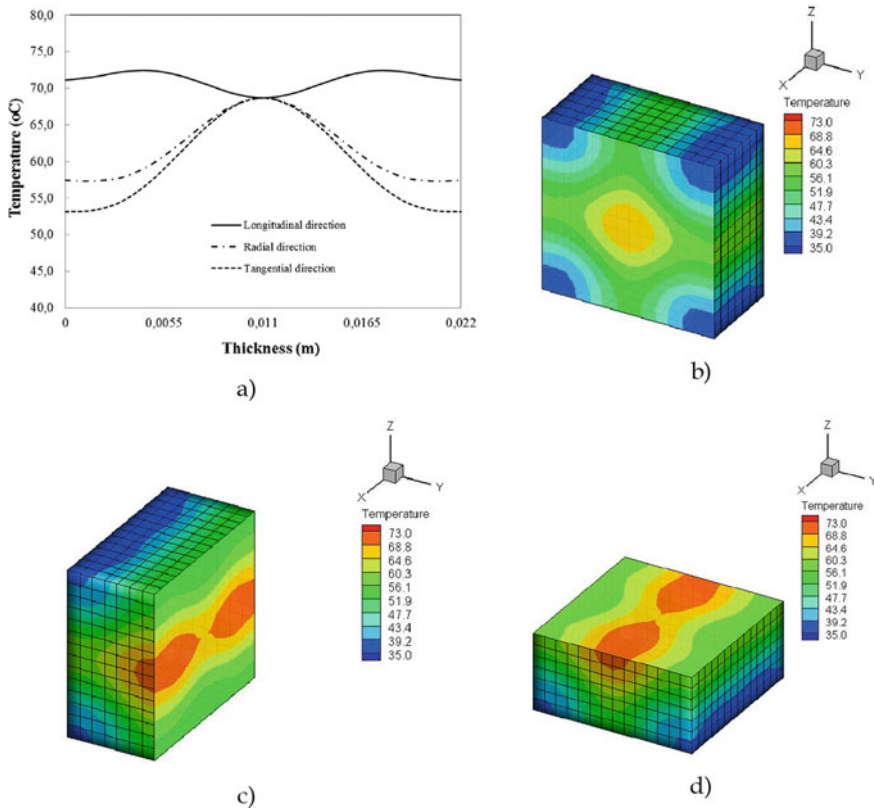


**Fig. 9** a Temperature profiles distribution and views of the temperature distribution at half-planes of symmetry of **b** longitudinal, **c** radial and **d** tangential direction for aspen trembling sample exposed to microwave at time = 200 s,  $I_0 = 1 \text{ W/cm}^2$ ,  $f = 2466 \text{ MHz}$ ,  $T_0 = -20 \text{ }^\circ\text{C}$

white birch, and sugar maple, respectively for initial temperatures of  $-15$ ,  $+0$  and  $15 \text{ }^\circ\text{C}$ . The percentage of disinfected sapwood is defined as the fraction of wood that reaches the temperature of  $56 \text{ }^\circ\text{C}$ . One can easily note that the required treatment time to reach 100% disinfection increases when the initial temperature decreases. On the other hand, the treatment time of complete disinfection by microwave energy is significantly higher when the initial temperature is below zero. This finding is explained by the accumulation of latent energy in the heating of the solid ice present in the material. Once exceeded, the material temperature increases more easily (thermal conductivity in the liquid region is high). Figure 15 summarizes various minimum times required to achieve 100% disinfection as a function of initial temperature and wood type for lower temperatures and higher temperatures. One can clearly see that the minimum time to achieve 100% disinfection depends strongly on the wood type and on the initial temperature. For example, at the initial temperature of  $-20 \text{ }^\circ\text{C}$ , this time is 262, 306 and 380 s for trembling aspen, white birch and sugar maple,

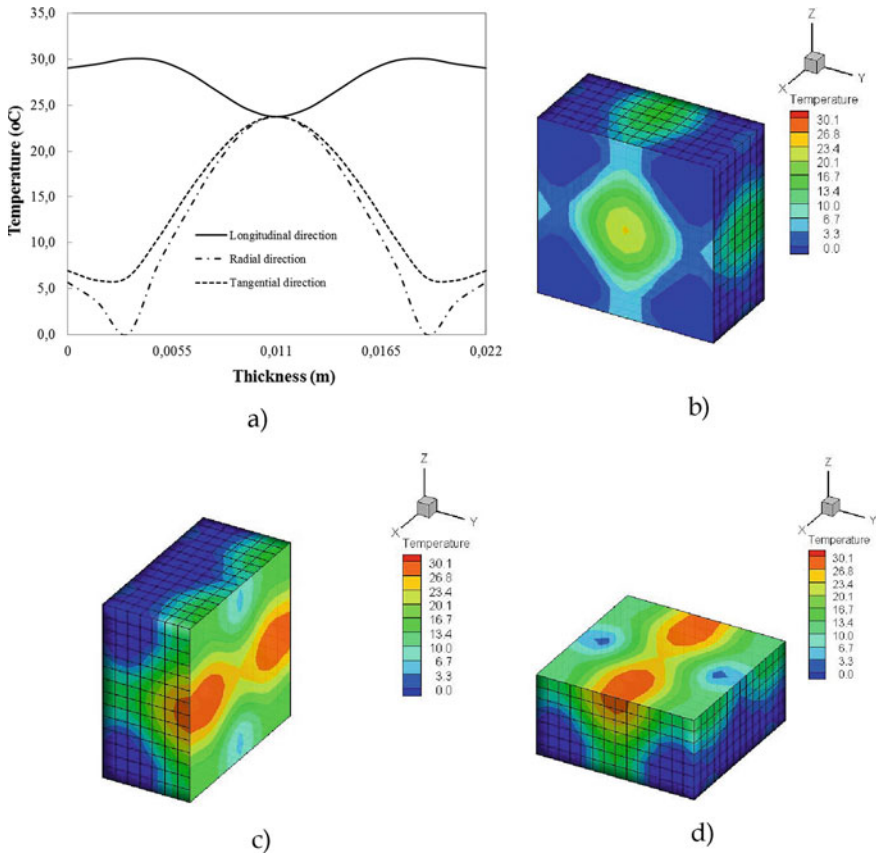


**Fig. 10** a Temperature profiles distribution and views of the temperature distribution at half-planes of symmetry of b longitudinal, c radial and d tangential direction for sugar maple sample exposed to microwave at time = 200 s,  $I_0 = 1 \text{ W/cm}^2$ ,  $f = 2466 \text{ MHz}$ ,  $T_0 = -20^\circ\text{C}$

respectively. At + 20 °C, this time is 101 s, 106 s and 132 s for trembling aspen, white birch and sugar maple, respectively.

As a note, the example presented in this chapter concerns the numerical estimation of the phytosanitary treatment time, using microwave energy, for three types of Canadian wood for a simple geometry. However, the approach proposed to model the heat equation in terms of anisotropic enthalpy of volume is, in our opinion, very robust and applicable, a priori, to any type of wood product (frozen or unfrozen). However, in cases where the product to be treated by microwaves is a multi-material with multi-orientation of the thermal conductivity matrices, it is then appropriate to use more appropriate approaches such as the one presented in (Erchiqui and Annasabi 2019). Moreover, this new approach, coupled with Maxwell’s equations, is under development.

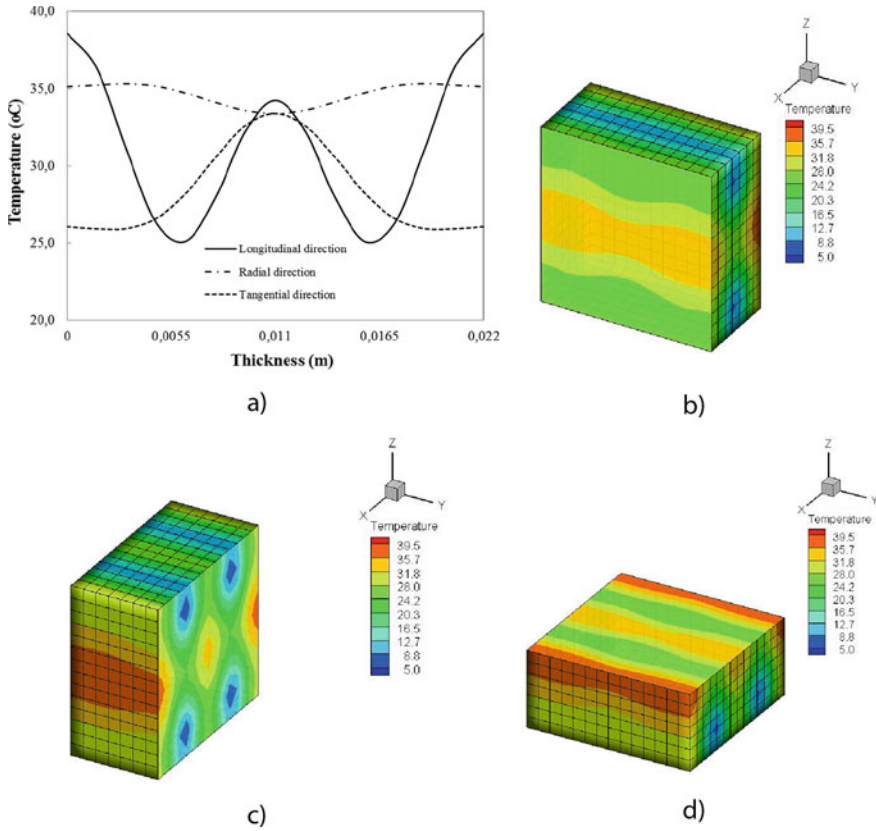


**Fig. 11** a Temperature profiles distribution and views of the temperature distribution at half-planes of symmetry of **b** longitudinal, **c** radial and **d** tangential direction, for white birch sample exposed to microwave at time = 200 s,  $I_0 = 1 \text{ W/cm}^2$ ,  $f = 2466 \text{ MHz}$ ,  $T_0 = -20 \text{ }^\circ\text{C}$

**Table 3** Density (MC = 131%, at ambient temperature)

Hardwood	Density (kg/m <sup>3</sup> )
Trembling aspen (TA)	808
White birch (WB)	1109
Sugar maple (SM)	1264

## 9 Conclusion

This chapter describes a numerical approach, based on the 3D finite element method, to estimate the time required to disinfect wood products (frozen or unfrozen). For this, the heat conduction equation in terms of anisotropic volume enthalpy is considered. The study concerns the estimation of the optimal time for the phytosanitary treatment of three species of Canadian wood by microwave in accordance with FAO

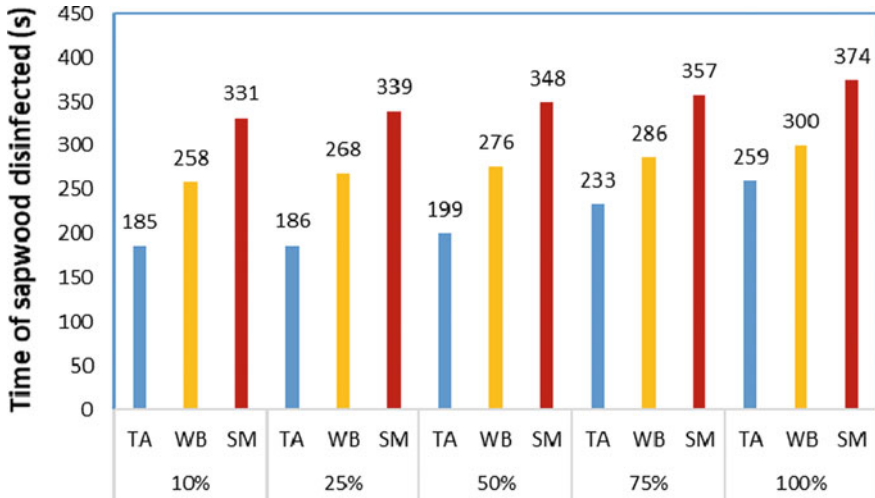
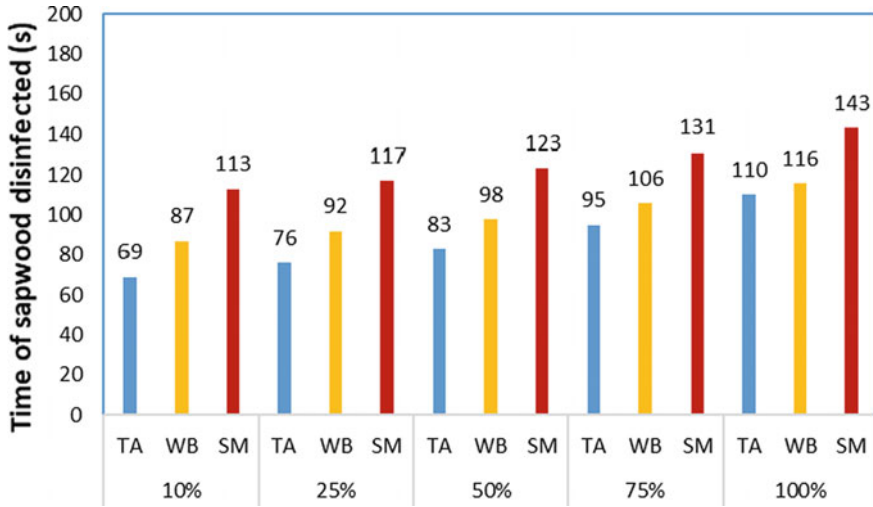


Fig. 12 Heat treatment by microwave energy ( $I_0 = 1 \text{ W/cm}^2$ ,  $f = 2466 \text{ MHz}$ ): Evolution of percentage sapwood disinfected (initial temperature is  $-15 \text{ }^\circ\text{C}$ )

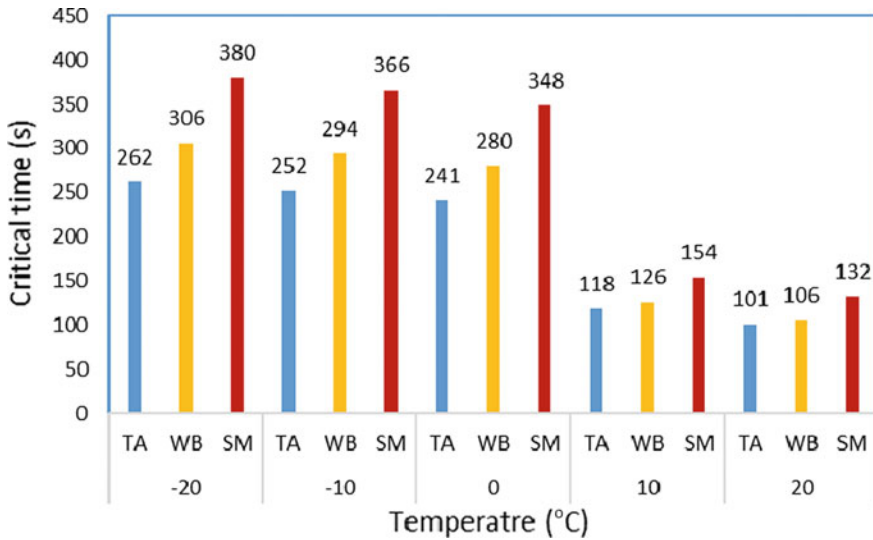


Fig. 13 Heat treatment by microwave energy ( $I_0 = 1 \text{ W/cm}^2$ ,  $f = 2466 \text{ MHz}$ ): Evolution of percentage sapwood disinfected (initial temperature is  $0 \text{ }^\circ\text{C}$ )

International Standard No. 15. The dielectric and thermophysical properties are a function of temperature, moisture content and orientation of the structure. From this modelling study, it was possible to accurately estimate the time required to reach the temperature recommended by the FAO International Standard. This makes it possible to optimize the time and thus the energy of the microwave heat treatment.



**Fig. 14** Heat treatment by microwave energy ( $I_0 = 1 \text{ W/cm}^2$ ,  $f = 2466 \text{ MHz}$ ): Evolution of percentage sapwood disinfected (initial temperature is  $15 \text{ }^\circ\text{C}$ )



**Fig. 15** Effect of initial temperature on critical time\* of heat treatment by microwave (MC = 131%, SG = 0.32). \*Time required for 100% disinfection. It can also be defined as:  $t_{crit} = \min(t_{crit}^{lon}, t_{crit}^{rad}, t_{crit}^{tan})$

More general cases will be studied in future work to establish the relationship between the treatment time, the initial temperature, the geometry of the sample wood and the physical properties of the wood.

## Appendix

### Electric Field in Parallel with One of the Three Principal Directions of the Wood

Rotation of the electric field vector  $\mathbf{E}$  on  $180^\circ$  does not change the dielectric properties of wood materials (Vyacheslav Komarov 2012). That is, L, R and T are the principal axes of anisotropy and the tensor  $\overline{\overline{\epsilon}}$  in Eq. (8) may be simplified as

$$\overline{\overline{\epsilon}} = \begin{bmatrix} \epsilon_L & 0 & 0 \\ 0 & \epsilon_R & 0 \\ 0 & 0 & \epsilon_T \end{bmatrix} = \begin{bmatrix} \epsilon'_L - j\epsilon''_L & 0 & 0 \\ 0 & \epsilon'_R - j\epsilon''_R & 0 \\ 0 & 0 & \epsilon'_T - j\epsilon''_T \end{bmatrix} \quad (60)$$

When  $\mathbf{E}$  is arbitrarily oriented in space and forms an angle  $\theta_1$  with L, angle  $\theta_2$  with R, and angle  $\theta_3$  with T, closed-form expressions for calculation of the relative dielectric constant,  $\epsilon'$ , and dielectric loss tangent,  $\tan \delta$ , is derived in (Vyacheslav Komarov 2012)

$$\epsilon' = (\epsilon'_L \cos^2 \theta_1 + \epsilon'_R \cos^2 \theta_2 + \epsilon'_T \cos^2 \theta_3) \quad (61)$$

$$\tan \delta = \tan \delta_L \cos^2 \theta_1 + \tan \delta_R \cos^2 \theta_2 + \tan \delta_T \cos^2 \theta_3 \quad (62)$$

with

$$\tan \delta_L = \frac{\epsilon''_L}{\epsilon'_L}, \quad \tan \delta_R = \frac{\epsilon''_R}{\epsilon'_R}, \quad \tan \delta_T = \frac{\epsilon''_T}{\epsilon'_T}, \quad (63)$$

If  $\mathbf{E}$  is parallel to one of the three principal directions of the sample wood ( $\theta_i = 0$ , for  $i = 1, 2$  or  $3$ ), the power dissipated per unit volume, given by Eq. (11), may be simplified as:

$$P_{wave} = -Re(\nabla \cdot \mathbf{S}) = \frac{\omega}{2} \epsilon_0 \epsilon''_d E_d^2 \quad (64)$$

$\epsilon''_d$  is the dielectric constant in the principal direction d (L, R or T).

## References

- Ayappa KG, Davis HT, Crapiste GE, Davis A, Gordan J (1991) Microwave heating: an evaluation of power formulations. *Chem Eng Sci* 46(4):1005–1016
- Basak T, Ayappa KG (1997) Analysis of microwave thawing of slabs with the effective heat capacity method. *Am Inst Chem Eng J* 43(7):1662–1674
- Bergman TL, Lavine A, Incropera FP, DeWitt DP (2011) *Fundamentals of heat and mass transfer—7th Edition* Incropera. Wiley Edition, ISBN 978-0-470-91323-9
- Bhattacharya M, Basak T, Ayappa KG (2002) A fixed-grid finite element based enthalpy formulation for generalized phase change problems: role of superficial mushy region. *Int J Heat Mass Transf* 45:4881–4898
- Brodie G (2007) Simultaneous heat and moisture diffusion during microwave heating of moist wood. *Appl Eng Agric* 23(2):179–187
- Bruch JC, Zyrolowski G (1974) Transient two-dimensional heat conduction problems solved by the finite element method. *Int J Numerical Method Eng* 8(3):481–494
- Chudinov BS (1965) Determination of mean effective thermal coefficients of wood. US Forest Service, Washington D.C.
- Coleman CJ (1990) The microwave heating of frozen substances. *Appl Math Model* 14:439–440
- Cooper PA, Ung T, Aucoin JP, Timusk C (1996) The potential for reuse of preservative treated utility poles removed from service. *Waste Manage Res* 14:263–279
- Dokainish MA, Subbraj K (1989) A survey of direct time-integration methods in computational structural dynamics. *Comput Struct* 32(6):1371–1386
- Erchiqui F (2013a) 3D numerical simulation of thawing frozen wood using microwave energy: frequency effect on the applicability of the Beer-Lambert Law. *Dry Technol* 31(11):1219–1233
- Erchiqui F (2013b) Analysis of power formulations for numerical thawing frozen wood using microwave energy. *Chem Eng Sci* 98:317–330
- Erchiqui F, Annasabi Z, Koubaa A, Slaoui-Hasnaoui F, Kaddami H (2013) Numerical modelling of microwave heating of frozen wood. *Can J Chem Eng* 9:1582–1589
- Erchiqui F, Annasabi Z (2019) 3D hybrid finite element enthalpy for anisotropic thermal conduction analysis. *Int J Heat Mass Trans* 136:1250–1264
- Erchiqui F, Kaddami H, Slaoui-Hasnaoui F, Koubaa (2020) A 3D finite element enthalpy method for analysis of phytosanitary treatment of wood by microwave. *Eur J Wood Wood Prod* 78:577–591
- Fields PG, White ND, G (2002) Alternatives to methyl bromide treatments for stored-product and quarantine insects. *Ann Revues Entomol* 47:331–359
- Flanders H (1973) Differentiation under the integral sign. *Am Math Monthly* 80 (6):615–627
- Food and Agriculture Organization, FAO (2009) Regulation of wood packaging material in international trade. International Standards for Phytosanitary Measures no 15 (ISPM 15). In: Food and Agriculture Organization of the United Nations, Secretariat of the International Plant Protection Convention, Rome, Italy
- Gašparík M, Barčík Š (2013) Impact of plasticization by microwave heating on the total deformation of beech wood. *BioResources* 8(4):6297–6308
- Gašparík M, Barčík Š (2014) Effect of plasticizing by microwave heating on bending characteristics of beech wood. *BioResources* 9(3):4808–4820
- Gašparík M, Gaff M (2013) Changes in temperature and moisture content in beech wood plasticized by microwave heating. *BioResources* 8(3):3372–3384
- Hansson L, Antti L (2003) The effect of microwave drying on Norway spruce woods: a comparison with conventional drying. *J Mater Process Technol* 141(1):41–50
- Hu H, Argyropoulos SA (1995a) Modelling of Stefan problems in complex configurations involving two different metals using the enthalpy method. *Modell Simul Mater Sci Eng* 3(1):53–64
- Hu H, Argyropoulos SA (1995b) Mathematical modeling and experimental measurements of moving boundary problems associated with exothermic heat of mixing. *Int J Heat Mass Transfer* 39:1005–1021
- Hollis CC (1983) *Theory of electromagnetic waves, A coordinate-free approach*. McGraw-Hill

- James WL (1975) Dielectric properties of wood and hardboard: variation with temperature, frequency moisture content, and grain orientation. USDA Forest Service Research Paper, Forest Products Laboratory
- Kaestner PA, Bååth LB (2005) Microwave polarimetry tomography of wood. *IEEE Sens J* 5(2):209–215
- Kanter KR (1975) The thermal properties of wood. *Derev Prom* 6(7):17–18
- Nedjar B (2002) (2002), An enthalpy-based finite element method for nonlinear heat problems involving phase change. *Comput Struct* 80(1):9–21
- Ni H, Datta AK (2002) Moisture as related to heating uniformity in microwave processing of solid foods. *J Food Process Eng* 22:367–382
- Norimoto M, Gril J (1989) Wood bending using microwave heating. *J Microw Power Electromagn Energy* 24(4):203–212. <https://doi.org/10.1080/08327823.1989.11688095>
- Norimoto M, Yamada T (1971) The dielectric properties of wood V, On the dielectric anisotropy in wood. *Wood Res* 51:12–32
- Nzokou P, Tourtellot S, Kamdem DP (2008a) Sanitization of logs infested by exotic pests: case study of the Emerald Ash Borer (*Agrilus planipennis* Fairmaire) treatments using conventional heat and microwave. USDA, Michigan Dept. of Natural Resources and the Dept. Of Forestry at Michigan State University
- Nzokou P, Tourtellot S, Kamdem DP (2008) Kiln and microwave heat treatment of logs infested by the emerald ash borer (*Agrilus planipennis* Fairmaire) (Coleoptera: Buprestidae). *Forest Prod J* 58(7):68–72
- Ohlsson T, Bengston N (1971) Microwave heating profile in foods—a comparison between heating and computer simulation. *Microwave Energy Appl Newsl* 6:3–8
- Oloyede A, Groombridge P (2000) The influence of microwave heating on the mechanical properties of wood. *J Mater Process Technol* 100(1–3):67–73. [https://doi.org/10.1016/S0924-0136\(99\)00454-9](https://doi.org/10.1016/S0924-0136(99)00454-9)Mori
- Panrie BJ, Ayappa KG, Davis HT, Davis EA, Gordon J (1991) Microwave thawing of cylinders. *A.I.Ch.E. J* 3:1789–1800
- Peralta PN, Bangi AP (2006) Finite element model for the heating of frozen wood. *Wood Fiber Sci* 38(2):359–364
- Peyskens E, Pourcq M, Stevens M, Schalck J (1984) Dielectric properties of softwood species at microwave frequencies. *Wood Sci Technol* 18:267–280
- Phillips TW, Halverson SL, Bigelow TS, Mbata GN, Ryas-Duarte P, Payton M, Halverson W, Forester S (2001) Microwave irradiation of flowing grain to control stored-product insects. In: *Proceeding of the annual international research conference on methyl bromide alternatives and emissions reductions*. San Diego, California, pp 121–122
- Pozar MD (2011) *Microwave engineering*, 4th edn. ISBN-13: 978-0470631553. Wiley
- Rattanadecho P (2006) The simulation of microwave heating of wood using a rectangular wave guide: influence of frequency and sample size. *Chem Eng Sci* 61:4798–4811
- Rattanadecho P, Suwannapum N (2009) Interactions between electromagnetic and thermal fields in microwave heating of hardened type I-cement paste using a rectangular waveguide (Influence of frequency and sample size). *J Heat Transfer* 131(8):1–12
- Simpson W, Tenwolde A (1999) Wood handbook-wood as an engineering material. Gen Tech Rep. FPL-GTR=113. Physical properties and moisture relations of wood. Chapter 3. U.S. Department of Agriculture, Forest Service, Forest Products Laboratory, Madison, WI
- Steinhagen HP, Harry W (1988) Enthalpy method to compute radial heating and thawing of logs. *Wood Fiber Sci* 20(4):451–421
- Swami S (1982) Microwave heating characteristics of simulated high moisture foods. M.S. Thesis. University of Massachusetts, USA
- Torgovnikov GI (1993) *Dielectric properties of Wood-based materials*. Springer-Verlag, Berlin, Germany



- United States Department of Agriculture (USDA) (2003) Importation of solid wood packaging material. Final environmental impact statement. Available at [https://www.aphis.usda.gov/plant\\_health/ea/downloads/swpmfeis.pdf](https://www.aphis.usda.gov/plant_health/ea/downloads/swpmfeis.pdf). Accessed Aug 2003
- USDA (1977) General technical report, Department of Agriculture Forest Service, thermal conductive properties of wood, green or dry, from  $-40^{\circ}$  to  $+100^{\circ}$  C: a literature review USDA forest service, FPL-9, U.S.
- Vyacheslav Komarov V (2012) Handbook of dielectric and thermal properties of materials at microwave frequency. Artech House, Boston. ASIN: B00AG0382Q
- Yemshanov D, Koch FH, McKenney DW, Downing MC, Sapio F (2009) Mapping invasive species risks with stochastic models: a cross-border United States-Canada application for *Sirex noctilio* fabricius. Risk Anal 29(6):868–884
- Zhu J, Kuznetsov AV, Sandeep KP (2007) Mathematical modelling of continuous flow microwave heating of liquids (effect of dielectric properties and design parameters). Int J Therm Sci 46:328–341
- Zielonka P, Gierlik E (1999) Temperature distribution during conventional and microwave wood heating. Holz Als Roh- Und Werkstoff 57:247–249